



Research paper

Performance assessment of a 20 MW photovoltaic power plant in a hot climate using real data and simulation tools

Said Bentouba^{a,*}, Mahmoud Bourouis^b, Nadjet Zioui^c, Arumugam Pirashanthan^a, Dhayalan Velauthapillai^a

^a Western Norway University of Applied Sciences, Faculty of Engineering and Science, Bergen, 5063, Norway

^b Department of Mechanical Engineering, Universitat Rovira i Virgili, Av. Països Catalans No. 26, 43007 Tarragona, Spain

^c Mechanical Engineering Department, University of Quebec at Trois-Rivieres, QC, Canada

ARTICLE INFO

Article history:

Received 8 July 2021

Received in revised form 11 October 2021

Accepted 13 October 2021

Available online 6 November 2021

Keywords:

Large-scale photovoltaic power plant

Real-time monitoring

HOMER pro

RETScreen

Hot climate

ABSTRACT

The present study aims to evaluate the aptness of two commercial simulators, HOMER Pro and RETScreen Expert, as predictors of the performance of a large-scale photovoltaic power plant designed to deliver up to 20 MW in a hot climate, for which 26 months of real operational data are available. The power plant is located in the province of Adrar in the south of Algeria and classified as one of the hot regions worldwide. Performance parameters were reference yield, performance ratio, capacity factor, temperature loss and statistical indicators. The results showed that photovoltaic power plant performance depends on cell technology, insolation, and environmental conditions, especially temperature. The deviations between the simulation results and real monitoring data were found to be smaller in the case of HOMER Pro simulation tool. The total annual energy supplied in 2018 by the power plant was 36364MWh, whereas RETScreen Expert predicted 42339 MWh, or about 14% more and HOMER Pro predicted 34508 MWh or about 5.1% less. The influence of temperature on the power plant output was strong, causing a 40% drop during the summer, due to the limitations of the polycrystalline cell technology. This needs to be considered in the design of future photovoltaic power plants to be operated in hot climates. HOMER Pro and RETScreen Expert predicted an average annual final yield of 5.128 h/day, a module efficiency of 15% and an inverter efficiency of 98%. The t statistics were 3.75 for HOMER Pro and 6.12 for RETScreen Expert. The analysis shows that the 20 MW photovoltaic plant in hot climate experiences high losses compared to an equivalent plant based on thin-film photovoltaic cells.

© 2021 The Authors. Published by Elsevier Ltd. This is an open access article under the CC BY license (<http://creativecommons.org/licenses/by/4.0/>).

1. Introduction

According to International Renewable Energy Agency (IRENA) figures, global renewable energy capacity grew to at least 260 gigawatts (GW) in 2020, an increase of nearly 50% compared to 2019, despite the slowdown due to the COVID-19 pandemic. Solar energy increased by 22% to 127 GW, and wind energy by 18% to 111 GW (IRENA, 2021). The increase in solar capacity is due largely to decreasing photovoltaic system costs. New Energy Outlook forecasts that the cost of solar electricity will fall by 60% over the next 20 years, and converting solar energy will become the cheapest way of producing electricity in most of the world by the year 2030 (Pothecary, 2016). Algeria depends heavily on revenue from the exportation of its massive oil and gas reserves, and over 90% of its electricity is generated from

these resources, placing its growing domestic demand for electricity under serious constraints. Meanwhile, the slump in oil prices since the third quarter of 2014 has nearly halved Algeria's foreign currency reserves. The Renewable Energy and Energy Efficiency Development Plan launched in 2011 and updated in 2015 emphasizes deployment of large-scale solar photovoltaic installations and onshore wind turbines, both made possible by decreasing costs as the technologies advance. Biomass, cogeneration and geothermal technologies were to be added until 2020. The goal of the program is to install 22 000 MW by 2030 (Fig. 1) which includes large grid-connected solar power plants with a total capacity of 13 500 MW (Algeria Ministry of Energy, 2021).

Photovoltaic system performance will depend on the technology used and on the climatic parameters of the power plant site. New-generation cells, components of the installation and the scale of the integration grid are being investigated to optimize the design and operation of these power plants. In this article, we compare the actual monitored performance of a photovoltaic power generator to simulations by HOMER Pro and RETScreen

* Corresponding author.

E-mail address: sben@hvl.no (S. Bentouba).

Algerian Renewable Program 2030

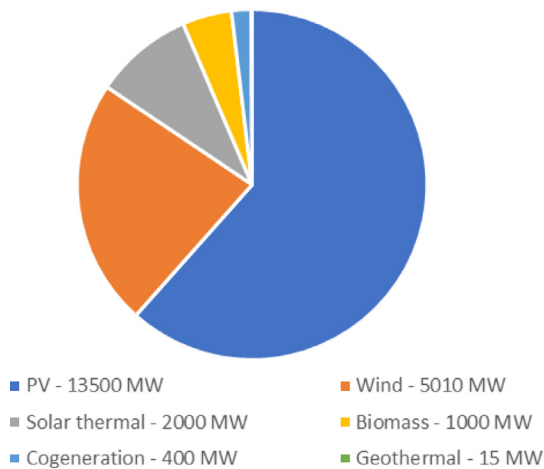


Fig. 1. The Algerian renewable energy program.

Expert. We also discuss the consequences of different internal component distributions and grid topologies.

An extensive review of the literature reveals a lack of information on the internal topology and integration of large-scale photovoltaic power plants into the power grid. Simulators are used to predict the energy production of the proposed system before integrating any large-scale variable renewable energy. We examine the aptness of RETScreen Expert and HOMER Pro using the case of a real 20 MW photovoltaic power plant operating in a hot climate. To the best of our knowledge, this is the first research article to describe, display and analyze in detail such a large mass of data obtained by monitoring power panel configuration, power production on hourly, daily, monthly, and yearly basis, insolation, temperature, module characteristics, and cable sections in an actual grid connection and to compare these to simulations. The data monitoring period was 26 months, from November 2016 to December 2018. The effectiveness of the system configuration is examined in terms of total energy generated, performance ratio, capacity factor and monthly system efficiency. In the second section of this article, the simulators are evaluated. The total amount of electrical energy generated and supplied to the load and the various types of power losses are predicted. Finally, the total energy flow through the whole system is calculated by predicting energy supplied to the load for one year and compared with data from real-time monitoring.

2. Related studies

Studies of large-scale photovoltaic power plants are relatively recent. A comparison of actual performance of a 5 MW grid-connected plant in South India with RETScreen predictions was recently performed (Sundaram et al., 2015), techno-economic analysis of grid-interactive solar photovoltaic (PV) projects implemented under the first phase of India's national solar mission (Purohit and Purohit, 2018). Use of novel algorithm relief attribute evaluator to evaluate the relative influences of solar radiation and back surface module temperature on predicted daily array yield of a 190 kW power plant using a radial basis function neural network for 26 Indian cities was presented in Yadav et al. (2018). A structured framework was examined for evaluating photovoltaic plant integration into weak distribution systems in grid connection studies in Susanto et al. (2018).

The analysis of performance ratio, yield energy, reference energy, capacity utilization factor and energy efficiency of different solar photovoltaic were also analyzed in Kumar and Kumar (2017). Furthermore, a review of the effects of dust accumulation and ambient temperature on PV performance in the Middle East and North Africa was explored in Hammad et al. (2018), assessment of 2.5 kW photovoltaic power generator performance under conditions of high losses due to environmental factors in southern Algeria were also surveyed in Necaibia et al. (2018). In cases studies, an analysis of the performance of grid-connected desert-type 1.4 kW photovoltaic plants under Muscat climatic conditions found that the total annual energy yield was 2217.6 kWh whereas the annual average daily reference yield, array yield and final yield were respectively 6.36 kWh/kWp-day, 4.56 kWh/kWp-day and 4.10 kWh/kWp-day and that energy production was 10% lower when the modules were left uncleaned, but no details were provided on the influence of temperature (Al-Badi, 2018). In an evaluation of design aspects of a 10 MW grid-connected photovoltaic power plant in terms of various types of power losses (temperature, internal network, power electronics, grid connected, etc.) and comparison with simulations by PV System and PV-GIS software, the final yield was 1.96–5.07 h/d and the annual performance ratio was 86.12% (Kumar and Sudhakar, 2015). In a study of a 5 MW photovoltaic power plant designed for 50 Iranian cities using RETScreen software, the highest capacity factor (26.1%) was found at Bushier and the lowest at Anzali (16.5%) for an average of 22.27% (Besarati et al., 2013). In a PV-GIS-based comparison of monocrystalline silicon, cadmium telluride (CdTe) and copper indium selenide (CIS) cells for 1 MW photoelectric solar power plants in 23 Serbian cities, CdTe was found most suitable, based on total annual production of electricity (Pavlović et al., 2013). In energy performance prediction and loss estimation for crystalline photovoltaic 200 kWp arrays in Northern India, the estimated degradation rate ranged from $-0.6/\text{year}$ to $-5/\text{year}$, light-induced degradation was $-2.5/\text{year}$ and the predicted energy losses ranged from -1757.724 to -14647.7 kWh/year (Kumar et al., 2019). The photovoltaic array efficiency, inverter efficiency and system efficiency of a 40 kWp GIPV system installed in India evaluated for one year were found to be 9.36%, 90.9% and 8.51% respectively (Satsangi et al., 2018). Based on the International Photovoltaic Project Model, the best scenario for a 12 kW photovoltaic power plant was the satisfaction of power demand by both solar (27%) and grid electricity (73%), with a minimal reduction in GHG emissions of 23 t of CO₂ per year (Rashwan et al., 2017). In a study of photovoltaic power plants (1523 kW and multi-MW) built in the best locations in the Canaries (Spain) and presumably well managed, simulation results deviated from measured specific yields (237 588 monthly energy values for 2005–2017) by less than 3% (Guerrero-Lemus et al., 2019). The model was also used to detect suboptimal plant designs and anomalous specific yields above the clear sky limit. Recommendations to avoid future anomalous specific yields were proposed. Analysis based on the standard IEC 61724 guidelines of the performance of six large photovoltaic power plants over several years of operation with different mounting topologies agreed largely with expected results by considering plant location in the South-Central Region of Spain, where the total system efficiency ranging from 10% to 12% (Martín-Martínez et al., 2019). A grid-connected 3 MW photovoltaic power plant located in Karnataka State (India) generated an average of 1372 kWh per year per kWp of installed capacity. This performance was found satisfactory based on the normalized comparison with installations in other countries (Padmavathi and Daniel, 2013). Components used in large-scale photovoltaic power plants including panels, converters and transformers as well as their distribution and the associated collection grid topologies have been reviewed (Cabrera-Tobar et al.,

Table 1
Daily solar radiation recorded in typical cities in the Algerian desert.

Province	Solar radiation in kWh/m ² per day	Sunshine in hours per day
Adrar	5.87	12.13
Bechar	5.38	12.12
Tamrasset	5.61	12.10
Tindouf	5.86	12.14

2016b). Technical, environmental and economic aspects of selecting 44 sites for 10 MW installed capacity grid-connected photovoltaic power plants in Saudi Arabia have been evaluated using RETScreen to predict energy production, greenhouse gas (GHG) emissions and financial parameters (Rehman et al., 2017). It was found that the town of Bisha was best suited due to insolation (intensity and duration). Design solutions for increasing the efficiency and yield of photovoltaic power generators mounted on a floating platform were tested in experiments that showed a considerable increase in efficiency due to positive tracking and reduced temperature effects (Cazzaniga et al., 2018). In a study of large-scale photovoltaic systems based on 1006.74 kWp crystalline silicon (c-Si) arrays in semi-arid climates of India, the degradation rate calculated from 4 years of operational data (using a linear least square fitting method) ranged from -0.30% to -0.17% starting from the third year of operation, which is within ranges reported previously in similar studies conducted in other regions (Kumar and Malvoni, 2019). A cost analysis of solar power systems located in Turkey shows that one of the most important financial factors blocking investment in renewable energy sources was high interest rates (Gürtürk, 2019). The growing scale photovoltaic power plants around the world and the importance of developing of grid codes for their integration has been discussed (Cabrera-Tobar et al., 2016a). The impact of wind direction on the overall performance of the utility-scale photovoltaic plant has been examined using six months of data collected from the Hadley solar plant in the United Kingdom from January 1 to July 1, 2017, which revealed that power production increased significantly under southerly wind conditions while keeping all other effective factors the same (Vasel and Iakovidis, 2017). An economic analysis of a photovoltaic and hydrogen turbine hybrid 100 MW power plant found that electricity could be provided at \$0.12/kWh in the average-case scenario, and \$0.16/kWh in the worst-case scenario, with payback periods of 13 years and 15 years respectively, based on an 8% interest rate (Ebaid et al., 2015). Finally, based on analysis of economic feasibility using HOMER, interior climatic zones would be preferred for photovoltaic/diesel hybrid systems (Suresh Kumar and Manoharan, 2014). Sensitivity analysis showed that the net present cost of such a system can be reduced. It is noteworthy that worldwide global solar energy capacity reached 714 GW in March 2021 (IRENA, 2021).

3. Methods and materials

3.1. Site description

African deserts, especially in Algeria, have immense potential for solar energy generation. The practically constant insolation amounts to 3500 h of annual sunshine, which is equivalent to more than 6000 trillion kWh. Almost all parts of Algeria receive 5–7 kWh of solar radiation per square meter per day (Bentouba and Bourouis, 2016). Table 1 shows the daily insolation in four Algerian provinces.

Table 2
Design parameters of the Adrar 20 MVp photovoltaic power plant.

Design parameter	Characteristics
Module type	Poly-crystalline silicon
Photovoltaic module efficiency	15%
Orientation and tilt	26.5°, south
Installation type	Fixed
Distance between photovoltaic rows	8 m
Inverters	500 kW
Transformers	1.250 kVA, 47–52 Hz, 315 V/31.5 kV

Table 3
Configuration of the Adrar 20 MWp power plant (SKTM, 2019).

Equipment	Number
245 Wp modules	81 840
1 MW subfields	20
Inverters	40
1250 kVA/630 kVA transformers	20

3.2. Description of the 20 MW photovoltaic power plant

The photovoltaic power plant studied in this article is situated in the southwest of Algeria, a region very rich in solar power potential due to its topography and low latitude. The Adrar station is the legal entity mandated to provide renewable energy in Algeria, where it has a capacity of 20 MWp and it is one of the seven photovoltaic power facilities built by the renewable energy subsidiary of the state-owned power provider Sonelgaz (SKTM) (SKTM, 2019). It covers a rectangular area about 1000 m long and 400 m wide about 0.3 km east of route CW N°73 (27°54'15.71"N and 0°18'45.25"W) as shown in Fig. 2. The axis of the site deviates by -58° from due south. The altitude is about 258 m. The site comprises 20 photovoltaic subfields of 1 MWp formed by a two-inverter conversion station and a transformer station. The entrance, command shelter and evacuation outpost are in the east central part of the site. The general layout, equipment, and operation of the main systems and components, the photovoltaic field (solar panels, load-bearing structures, assembly boxes, cabling, conversion stations and transformer stations are described below. Design parameters of the Adrar 20 MVp photovoltaic power plant are presented in Table 2. The energy produced is intended to increase the reliability of the local electricity grid, which supplies power to about 27 100 houses.

3.3. Description of the subfields and modules

To achieve the desired power, the photovoltaic plant architecture factors in the constraints of compatibility with inverter characteristics were summarized in Table 3.

The panels contain Yingli type solar cells made from blocks of poly-crystallized silicon. These cells cost less to manufacture than monocrystalline cells, but their energy loss is considerable in hot climates (Tossa et al., 2016). With 81 840 modules rated 245 Wp, the installed power generation capacity is 20.0508 MWp or 1.003 MWp per subfield of 4092 modules. Each subfield is equipped with two inverters and a step-up transformer. The inverters (output voltage 315 V AC) are connected to the low-voltage side via AC cables to the 1.250 kVA transformer, which raises the voltage to 31.5 kV. The 20 subfields are connected to the 30 kV evacuation station. The electricity produced is evacuated by a 30 kV overhead line connected to the local grid as shown in Fig. 3.

3.3.1. The 1 MW subfields

Each subfield is equipped with three-level grouping boxes. The photovoltaic modules are connected to 500 kW inverter cabinets through junction boxes (level 1), parallel boxes (level



Fig. 2. Aerial view of the Adrar solar (photovoltaic) power plant (SKTM, 2019).

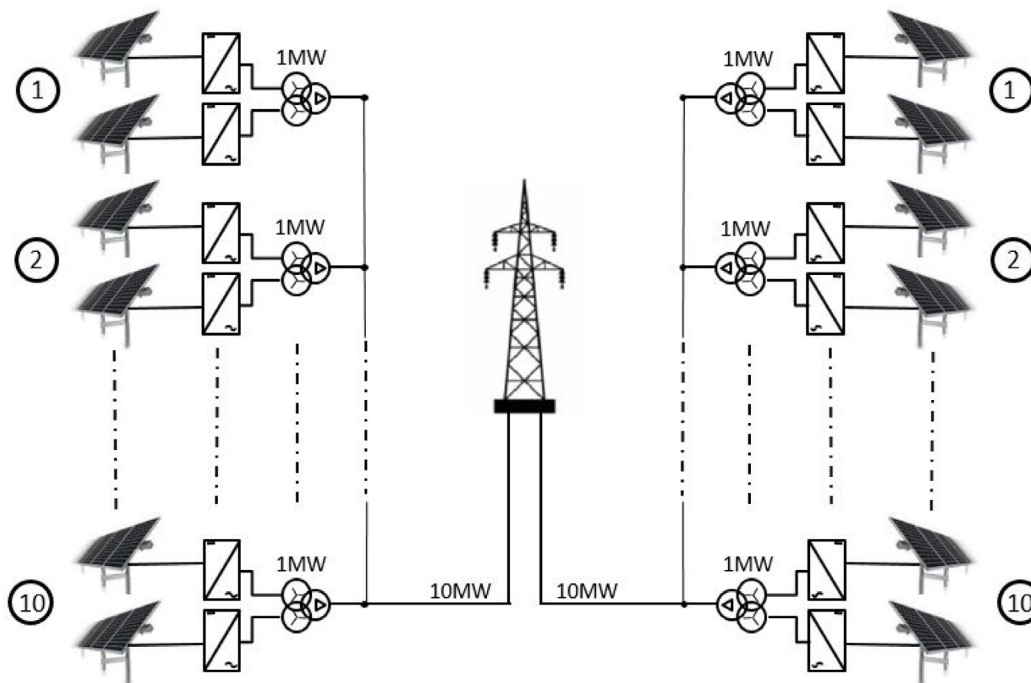


Fig. 3. General scheme of the Adrar 20 MW power plant connected to the grid.

2) and general boxes (level 3). Direct current is converted into alternating current and sent to the transformer station. The three-stage grouping boxes reduce the total length of the DC cables and ohmic losses therein and improve the efficiency of power generation throughout the plant as shown in Fig. 4.

3.3.2. Transformer substation

The transformer substations of all subfields are connected by 31.5 kV medium-voltage cables forming two ring circuits each connecting 10 substations, and then to the 30 kV evacuation grid. Each ring circuit reduces the length of the medium-voltage AC

cables and hence losses therein. A subfield or transformer substation failure does not affect production by the other subfields, thus ensuring power deliverability.

For each 1 MW subfield, a transformer substation of 1.250 kVA is planned to include:

- A dry main transformer of $31.5 \pm 2 \times 2.5\%/0.315/0.315$ kV.
- Three 31.5 kV cells from the ring circuit to the SF6 isolation.

3.4. Photovoltaic modules

The characteristics of the Yingli 245 W polysilicon photovoltaic solar modules chosen by SKTM are shown in Table 4.

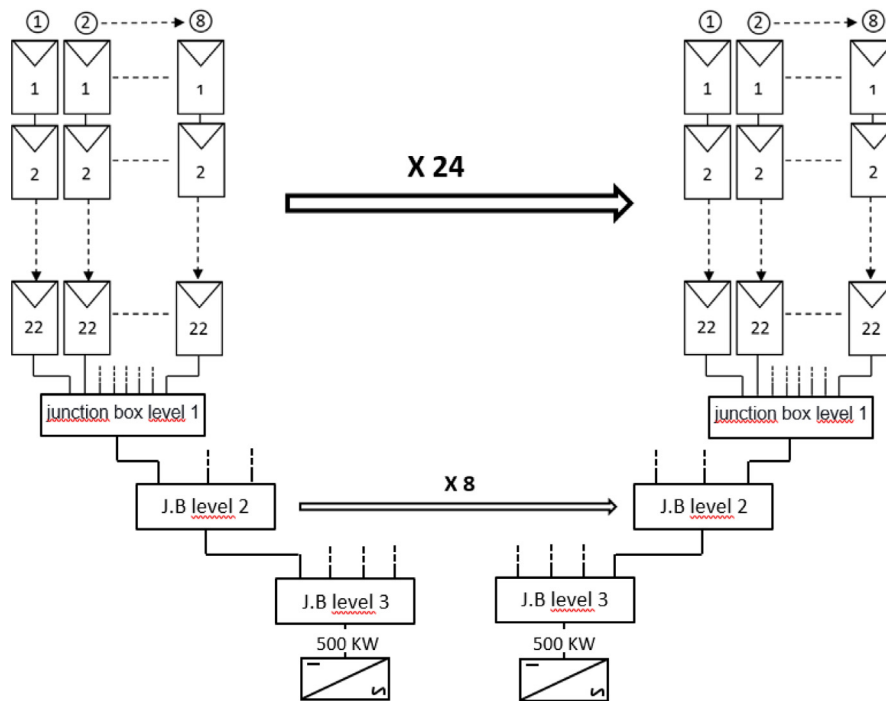


Fig. 4. Schematic outline of a 1 MW subfield in the Adrar photovoltaic power plant.

Table 4

Power plant panel characteristics (SKTM, 2019).

Module type	Yingli Solar YL245-29b
Measured power	245 W (± 5 W)
Measured current	8.28 A
Open-circuit voltage	37.7 V
I (continuous current)	8.83 A (DC)
Fire resistance class	C
Application class	A
Nominal operating cell temperature NOCT °C	46 \pm 2
Temperature coefficient of Pmax γ %/°C	-0.45

3.5. Choice of optimal inclination angle

The angle of inclination of the panels is not adjusted throughout the year. The angle that maximizes the annual irradiation is 27° as shown in Fig. 5, which was calculated using HOMER Pro based on the curve of monthly data.

3.6. The distance between module rows

The panels must also be spaced optimally to avoid shading (Radziemska and Klugmann, 2002). This spacing was determined again using HOMER Pro software, which considers the daily change in the path of the sun throughout the year, independently of the exact site location and plant layout. The optimal spacing between the rows of the north–south facing panels based on the actual field size was 8 m and the distance is the same for other photovoltaic power plants installed in this hot region.

3.7. Main parameters

Two photovoltaic strings (22 panels) are installed per supporting structure in a 2 x 11 panel matrix in landscape orientation. The maximal height of the supporting structures is approximately 2.37 m for the panel used in the Adrar power plant with the size of 1.650 mm x 990 mm x 40 mm.

3.8. Direct current grouping boxes

The modules are connected via grouping boxes. These three-level direct-current connection boxes are included in the schematic representation of power plant architecture.

3.8.1. Junction boxes (level 1)

The 24 level-1 direct-current junction boxes (1 for each 1 MW subfield) connect the photovoltaic module chains and transmit the produced power to the parallel boxes (level 2). Each has 8 inputs and 1 output installed on the load-bearing structures of the panels. They thus each can receive 8 module chains. Each input (two polarities) is equipped with a current fuse protection. Each chain of 22 modules is connected to one junction box, as shown in Fig. 4.

$$V_{J11} = N_s * V_{mpp} \tag{1}$$

$$I_{J11} = I_{mpp} * N_p \tag{2}$$

3.8.2. Parallel boxes (level 2)

The level-2 parallel boxes connect the level-1 junction boxes to the level-3 general boxes. A total of 8 parallel DC lightning protection boxes with 4 inputs and 1 output are installed per subfield. Parallel boxes contain 3 level-1 junction box outputs each.

$$V_{J12} = N_s * V_{mpp} \tag{3}$$

$$I_{J12} = I_{J11} * 3 \tag{4}$$

3.8.3. General boxes (level 3)

A general box installed at the entrance of each inverter (500 kW) ensures the connection between the appropriate level-2 parallel box and the solar inverter. Two level-3 general boxes (level 3) with 4 inputs and 4 outputs per subfield are installed in the conversion station. Each general box contains 4 level-2 (parallel box) outputs, as implied in Eqs. (5) and (6).

$$V_{J13} = N_s * V_{mpp} \tag{5}$$

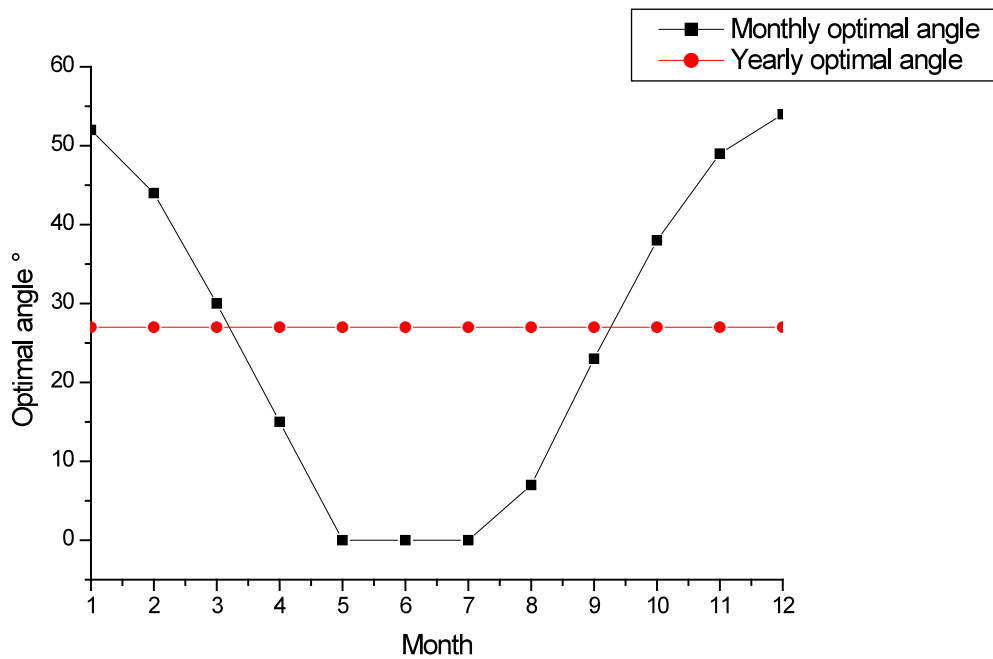


Fig. 5. Calculation of the optimal angle for solar panels at the Adrar power plant.

$$I_{j13} = I_{j12} * 4 \tag{6}$$

The general boxes are equipped with four inputs (two polarities), four outputs (two polarities) up to 240 mm² and 4 DC fuse switches for system protection.

Each inverter (500 kW) is connected to a level-3 junction which comprises 4 level-2 junctions and each of which is connected to 3 level-1 junctions. Each 1 MW subfield thus comprises a total of 24 junctions, 6 junction boxes containing 7 chains of 22 modules and 18 junction boxes with 8 chains of 22 modules. A one-megawatt subfield thus comprises 4092 panels. All junctions are equipped with a lightning arrester (two-polarity lightning protection) to protect the electrical system against direct shock and inductive shock and with a monitor to control the current and voltage on each string. These structures are inside the box. Real-time data can be sent via an RS485 serial cable. The box housing is made of metal to ensure long-lasting and stable operation in an outdoor environment.

3.9. Cabling

The lengths of the cables from the panels to the transformers (Table 5) are calculated from the three-level single-line diagram of the grouping boxes, the ring circuit connection of the transformer stations and the layout of the photovoltaic fields on the site.

3.10. Inverters

The inverter is an electronic device that converts direct current produced by photovoltaic modules to alternating current using control and protection circuitry. It can accept the maximal current and voltage produced by the photovoltaic field. The power plant is equipped with 40 inverters of 500 kW DC/AC, 2 per subfield. The ~520–820 VDC input range ensures AC output voltage stability with a maximal current of 1100 A at high efficiency (maximum ≥ 98.5%). The DC side of the inverters has 4 two-polarity inputs each equipped with direct current fuse protection, a general disconnect switch and a DC lightning arrester. The technical specifications of the inverters are shown in Table 6.

Table 5

Cable dimensions in the Adrar 20 MW power plant.

Equipment	Diameter	Length
Junction box (level 1)	4 mm ²	91.5 km
Parallel box (level 2)	≥ 70 mm ²	30.5 km
General box (level 3)	240 mm ²	27.0 km
3 three-core AC cables for connection between the AC side of the inverter and the low-voltage side of the main transformer. Aluminum section = 3 * 240 mm ²		
31.5 kV single-core cable to the aluminum core with XLPE insulation for ring circuits between transformer stations and the evacuation outpost	3 * 240 mm ²	1.8 km

Table 6

Main characteristics of the inverters (DC ≥ AC converters) (SKTM, 2019).

Inverter	Specification
Rated AC power	500 kW
Max. output power	550 kVA
Output frequency range	47~52 Hz
Maximum efficiency	98.5%
Max. DC input voltage	1000 V
Max. DC input current	1100 A
MPPT voltage	~500–820 (VDC)
Voltage on cable output	315 (VAC)
Power factor	~0.9–1
Harmonic distortion rate [%]	<IP20
Envelope protection level	3% (nominal power)
Ambient temperature range	~30–55 °C

3.11. Transformers

The transformer substation is used to raise the output voltage of the two inverters and send the electricity generated to the evacuation outpost. There are 20 transformers in the power plant as one transformer substation for each 1 MWp subfield. SUNTUN manufactured the 1250 kVA class transformers to step up the low-voltage output of the inverters to a medium voltage of 30 kV.

3.12. Photovoltaic penetration

The cumulative photovoltaic power generation capacity installed in Algeria was 448 MW at the end of 2019 (IRENA, 2021), which was still less than 3% of peak demand. On July 12th 2021, at 14:30, a new historic peak in power consumption estimated at 16065 MW was recorded <https://www.radioalgerie.dz/news/fr/article/20210713/214632.html>, <http://www.aps.dz/economie/91571-electricite-un-nouveau-record-de-consommation>. In its quest to meet the growing demand for electricity using sustainable resources, Algeria could follow the example of its southern region, which now has a micro-grid network comprising 7 photovoltaic power plants each generating 33 MW, one wind farm generating 10.2 MW, albeit more than 500 MW generated by fossil fuels (Table 7). Photovoltaic electricity now powers 27 100 houses in the region, plus hospitals, schools and a university.

4. Methodology

Twenty-two months of energy production data were obtained from the AC billing meters provided by the distribution system operator SKTM (renewable energy subsidiary of the state-owned power provider Sonelgaz), which logs data every 2 min. The uncertainty of the AC billing meters is small (0.2–0.5%). The data combine production from all large photovoltaic power plants built in Adrar. The analysis and conclusion from this large and optimized facility can be considered as a reference for calibrating new projects to be built in similar hot climatic regions of Africa and MENA. It is important to analyze data from photovoltaic power plants that inject electricity into the grid rather than with installed capacity.

The parameters of solar energy systems and components thereof have been established by the International Energy Agency (IEA) Photovoltaic Power Systems Program and are described in IEC standard 61724 (Şenol et al., 2016). Those most relevant to our analysis are energy output, array yield, final yield, reference yield, module efficiency, inverter efficiency, system efficiency, energy loss (array capture loss and system loss), performance ratio and capacity factor. These normalized indicators serve as key comparators for evaluating the performance of this large-scale photovoltaic power plant (Marion et al., 2005; Al-Badi, 2018; Padmavathi and Daniel, 2013).

These performance parameters allow the detection of operational problems, which facilitate the comparison of systems. However, that may differ concerning design, technology, or geographic location, and validate models for system performance estimation during the design phase.

4.1. Final yield rating (Y_f)

The final yield rating is the energy produced by the field divided by the peak power of the array. It represents the number of hours that the array would need to operate at its rated power to provide the same energy as at peak power (Marion et al., 2005).

$$Y_f = \frac{\text{actual output AC energy}}{\text{rated array capacity}} = \frac{E_{AC}}{P_{\text{rated}}} \quad (\text{hours}) \quad (7)$$

P_{rated} is the rated capacity of the array in kW.
 E_{AC} is actual array output energy in kWh.

4.2. Reference yield Y_r

The reference yield is the total in-plane irradiance divided by the reference irradiance. It represents the number of peak

sun hours or insolation in units of kWh/m² and defines the solar radiation resource potentially available to the system. It is a function of photovoltaic array location and orientation and month-to-month and year-to-year weather variability (Marion et al., 2005):

$$Y_r = \int_{t_1}^{t_2} \frac{(\text{solar radiation}) dt}{1000} \quad (8)$$

where t_1 and t_2 are the instantaneous start and end times for each data record and the integral gives the in-plane irradiation of the array over that time interval.

$$Y_r = \frac{H}{G_{\text{ref}}} \quad (9)$$

H is the derived array plane insolation in Wh/m².
 G_{ref} is the reference irradiance at STC (1000 W/m²)

4.3. Performance ratio

The performance ratio indicates the degree of utilization of a photovoltaic system as a whole (International Electrotechnical Commission, 1998). It is the ratio of the normalized parameters Y_f and Y_r , that is, the solar energy converted and utilized as AC current divided by the energy that could have been generated under ideal conditions of operation and utilization (Padmavathi and Daniel, 2013).

$$PR = \frac{Y_f}{Y_r} \quad (10)$$

4.4. Capacity factor

The capacity factor is defined as the ratio of the actual energy output in AC current to the amount of energy that the system would generate if it operated at nominal power continuously throughout the year (for 8760 h).

$$CF = \frac{\text{actual energy output}}{8760 \cdot \text{system rated power}} = \frac{E_{AC}}{P_{\text{nom}} \times 24} \times 100 \quad (11)$$

The capacity factor represents the energy delivered by an electrical power generating system, whether conventional or renewable-resource-based (ElhadjSidi et al., 2016).

$$\text{Photovoltaic efficiency, } \tau_{pv} = \frac{E_{DC}}{\text{PV area} \cdot \text{irradiation}} \quad (12)$$

$$\text{Inverter efficiency, } \tau_{in} = \frac{\text{inverter export}}{E_{DC}} \quad (13)$$

$$\text{System efficiency, } \tau_s = \frac{E_{AC}}{\text{PV area} \cdot \text{irradiation}} \quad (14)$$

The units of the terms E_{DC} , inverter export and E_{AC} are kWh. The units of irradiation are kWh/m². The capacity factor is technically more suitable for power plants that run continuously. Like most renewable energy systems, solar photovoltaic power plants run intermittently, since insolation is never constant or even available for 24 h. The CF ranges from 0.05 to 0.30 for photovoltaic power plants. This performance measurement is unavoidable in comparison with conventional power generation.

5. Results and analysis

5.1. Data monitoring system

The performance of the photovoltaic plant is assessed using a huge database logged via a sensor-based system that monitors the electrical status of the panels, junction boxes, inverters, and transformers as well as the local weather conditions. The SCADA

Table 7
Topology of the electrical micro-grid in the Adrar/In Salah/Timimoun region of Algeria (SKTM, 2019).

Province	Fossil-fuel power plants (number × MW)	Total MW	Renewable energy power plants
Adrar	4 × 25 + 2 × 8	116	20 MW photovoltaic
In Saleh	4 × 24	96	6 photovoltaic
Kabertan	2 × 20	40	10.2 MW wind + 3 MW photovoltaic
Timimoun	2 × 20 + 2 × 25	90	9 MW photovoltaic
Zaouit Kounta	8 × 20	160	6 MW photovoltaic
Reggane	0	0	6 MW photovoltaic
Aoulef	0	0	6 MW photovoltaic
Total	24	502	66.2 MW photovoltaic+wind

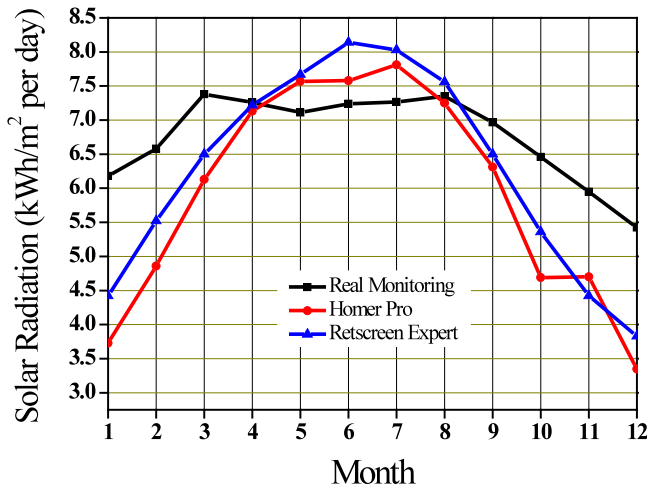


Fig. 6. Solar radiation, monitored on the ground and calculated from satellite data.

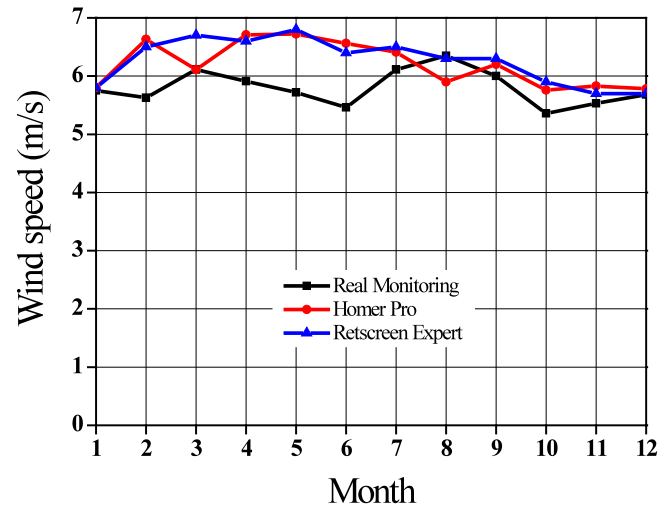


Fig. 7. Wind speed, monitored by weather stations and calculated from satellite data.

control command system links a central control room to the power plant, annexed installations, and the 30 kV substation. In addition to monitoring and control, the system plays a central role in communication. Any equipment operation that is not under its authority is still monitored, making all gatherable information available on its network. The power plant runs all the time except when stopped to solve technical problems. Global horizontal irradiance (GHI), direct normal irradiance (DNI), ambient temperature (T_a), DC and AC electrical energy generated (E_{DC} and E_{AC}) are measured instantaneously at 2-minute intervals. Wireless transmitters are used to log data from wind speed and relative humidity sensors.

5.2. Meteorological data

Irradiance, temperature and wind speed data were collected from November 1, 2016 through December 31, 2018 (two years and two months) via SCADA. RETScreen weather data were produced by Environment Canada and HOMER Pro by NASA. The monthly variation of average daily insolation on the panels (monitoring, RETScreen Expert and HOMER Pro) is shown in Fig. 6. Real data and software data differed somewhat. The measured average insolation varied from 5.422 kWh/m²/d in December to 7.34 kWh/m²/d in September compared to 3.36 kWh/m²/d and 7.82 kWh/m²/d (July) for HOMER Pro and 3.83 kWh/m²/d to 8.14 kWh/m²/d (June) for RETScreen Expert. HOMER Pro and RETScreen use algorithms to calculate insolation from satellite data. In any case, insolation was found to be consistently higher in the months of March through August than September through February. It was greater than 7 kWh/m² per day for the six months of Spring and Summer.

The comparisons of wind speed and of temperature data from the three sources are shown in Figs. 7 and 8. Again, monitoring

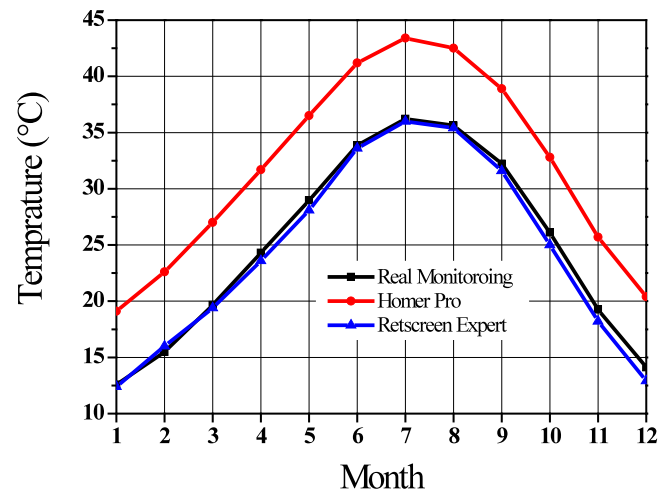


Fig. 8. Temperature, monitored by weather stations and calculated from satellite data.

and software calculation give differing profiles. In these cases, the real weather data were obtained from local weather stations near the power plant.

The average daily ambient temperature measured by the SKTM weather station in the power plant varied from 19.1 °C in January to 43.4 °C in July. During the monitored period, module temperatures reached 69.73 °C at an irradiance of 1024 W/m² and a wind speed of 5.7 m/s. Wind over the modules lowers the cell operating temperature. The average wind speed varied from 5.63 m/s in February to 6.11 m/s in July (Fig. 7). Although the profiles are the same, HOMER Pro disagrees considerably with RETScreen and the

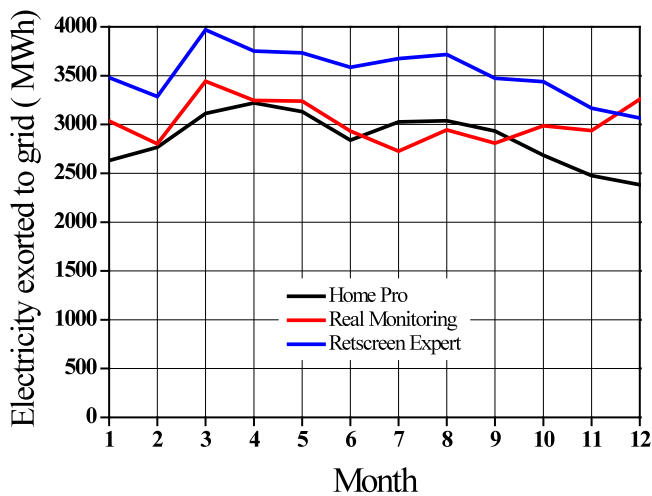


Fig. 9. Monthly electricity production, monitored and calculated by HOMER Pro and RETScreen Expert.

real data. Air temperature is correlated weakly with electricity production.

5.3. Electricity production

The monthly production of electricity is shown in Fig. 9. Monitoring shows 2725.72 MW in July versus 3442.875 MWh in March. HOMER Pro calculated 2382.54 MWh in December and 3130.905 MW in May and RETScreen Expert gave 3066.45 MWh in December and 3969.52 MWh in March. Annual production recorded by monitoring was 36,363.875 MWh versus 34241.24 MWh calculated by HOMER Pro and 42 338.57 MWh by RETScreen Expert. HOMER Pro is thus closer to reality. In all three cases, the average daily energy output was higher in March through November than in January through February.

Electrical energy output was essentially proportional to daily average insolation, as shown in Fig. 10 for monitoring data and in Fig. 11 for HOMER Pro.

The linearity of the relationship between insolation and electricity production is apparent when a winter day is compared to a summer day (Figs. 12 and 13). RETScreen Expert could not be compared since it generated only monthly and yearly data.

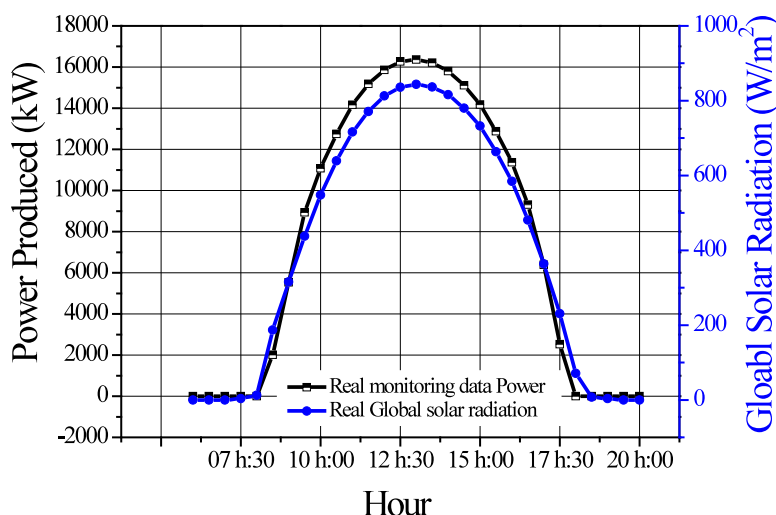


Fig. 10. Monitored daily production of electricity versus insolation during winter days.

Table 8

Analysis of power plant performance for the year 2017 (based on real data).

Month (2017)	Y_f	Performance ratio	Capacity factor
1	4.847903	78.44504	20.1996
2	4.619643	70.20734	19.24851
3	5.000194	67.7533	20.83414
4	5.296867	72.9596	22.07028
5	5.21129	73.29522	21.71371
6	5.029133	69.4814	20.95472
7	4.652387	64.02691	19.38495
8	5.125806	69.73981	21.35753
9	4.94025	70.92863	20.58438
10	5.444274	84.3054	22.68448
11	5.01975	84.40527	20.91563
12	4.977581	91.80849	20.73992

5.4. The influence of temperature

As shown in Figs. 14 and 15, the temperature measured in the installation lags daily power output, especially in the winter. Despite the long hours of insolation, the power loss is huge in the summer because of the climatic conditions and the choice of polycrystalline silicon photoelectric cells.

5.5. HOMER Pro and RETScreen system configuration

HOMER Pro defines simulation parameters in more detail than RETScreen Expert. In our case study, it was close to actual monitoring data. In addition, it simulates a viable system for all possible combinations of necessary equipment considering the case where no electrical energy storage is planned like our 20 MW photovoltaic power plant. HOMER simulates the operation of the photovoltaic power plant for a whole year, in time steps from one minute to one hour. All the electricity produced is sold to the grid, as shown in Fig. 16. In general, HOMER Pro can model photovoltaic systems that combine any type of conventional energy, renewable energy, storage, and load management, making decisions reliable, so that any system can be designed consistently.

HOMER Pro calculations of yearly solar radiation, grid sales, inverter input, inverter output, power output, ambient and cell temperature, and total renewable energy output are represented in Figs. 17 and 18.

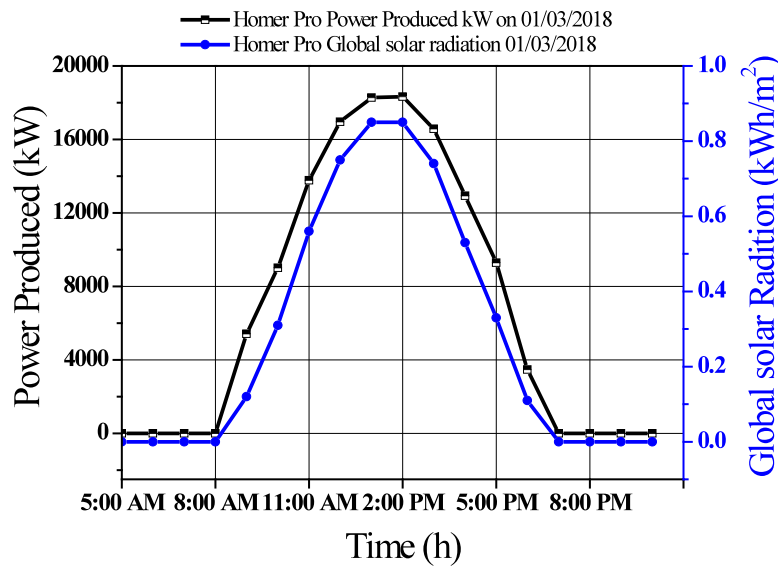


Fig. 11. HOMER-pro-calculated daily production of electricity versus insolation during winter days.

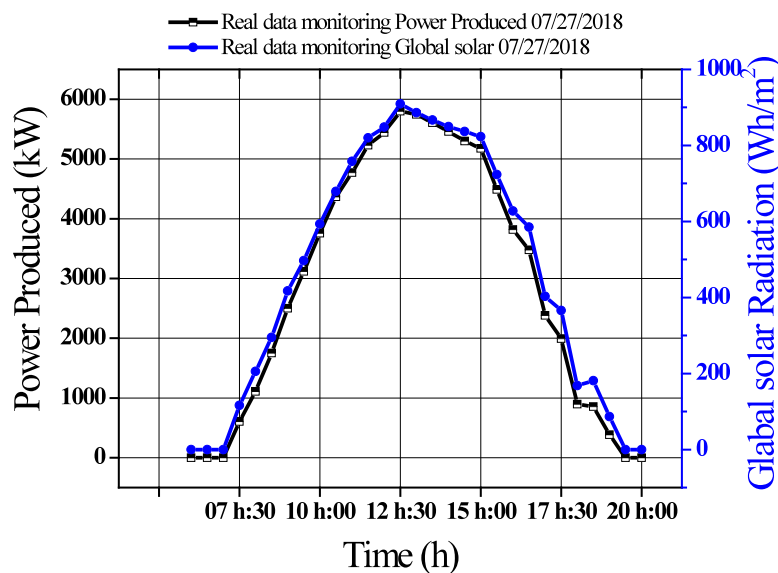


Fig. 12. Monitored daily production of electricity versus insolation during summer days.

5.6. Performance analysis

The performance of the power plant is assessed using the AC performance ratio, the overall system efficiency, and the capacity factor. In addition, the various capture loss parameters such as temperature provide valuable information about the magnitude of losses (see Tables 8 and 9).

Fig. 19 shows the monthly variation of the electrical energy delivery capacity factor as determined from the power plant monitoring system and is calculated by the software. The HOMER Pro calculations track the real data quite closely except for November, December, and January.

The average daily yield is directly proportional to the average daily insolation, varying from 4.3 h/d in January to 5.7 h/d in March based on measurement and from 4.9 h/day in January to 5.4 h/day in April based on a calculation by HOMER Pro as shown in Fig. 20. For most of the year, RETScreen Expert overestimated it, especially in the summer. The yield was proportional to electricity production and the daily average array yield and followed the

Table 9

Analysis of power plant performance for the year 2018 (based on real data).

Month (2018)	Y _f	Performance ratio	Capacity factor
1	4.895194	79.21025	20.39664
2	5.003857	76.04646	20.8494
3	5.553024	75.24423	23.1376
4	5.41175	74.54201	22.54896
5	5.22629	73.50619	21.77621
6	4.888833	67.54305	20.37014
7	4.396323	60.5029	18.31801
8	4.75029	64.63068	19.79288
9	4.681875	67.21906	19.50781
10	4.818629	74.61719	20.07762
11	4.89675	82.33707	20.40313
12	5.254105	96.90881	21.8921

trend of the reference yield Y_r. For all months of the monitoring period, there is a difference between average reference yield and system yield. This difference was expected, due to DC/AC conversion losses produced in the inverter.

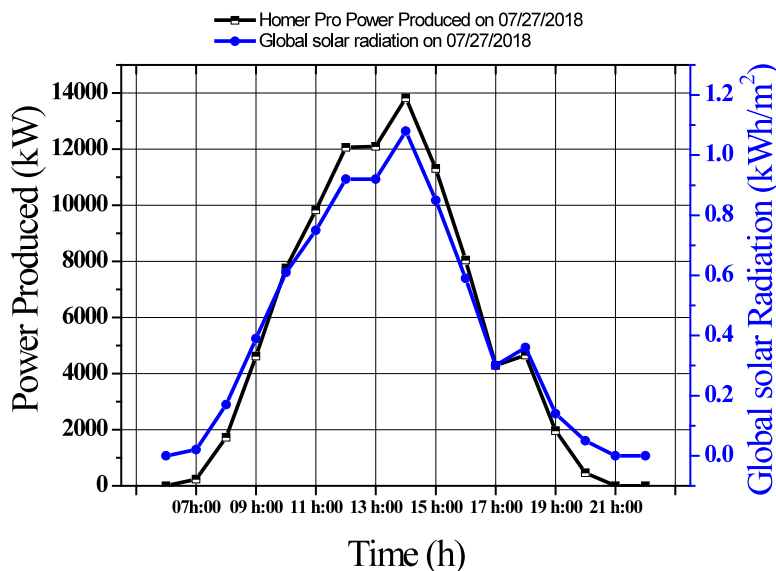


Fig. 13. HOMER-pro-calculated daily production of electricity versus insolation during summer days.

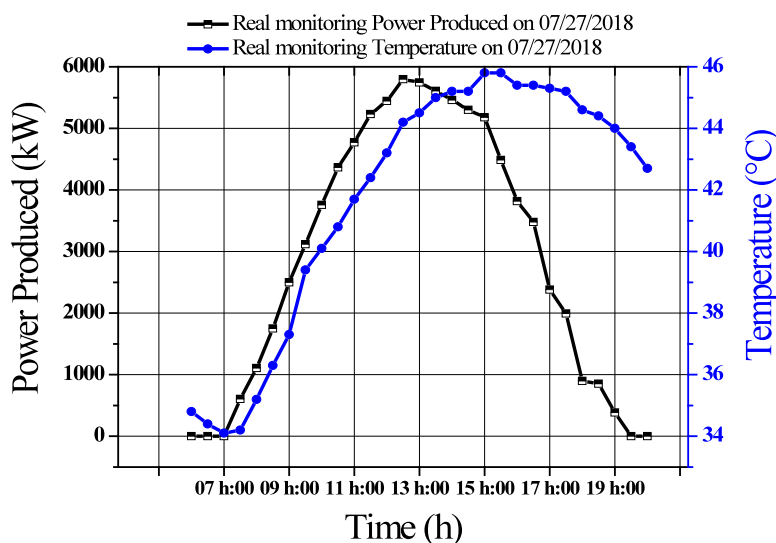


Fig. 14. Photovoltaic power output and ambient temperature measured on a typical summer day.

As predictors of the performance ratio (Fig. 21), HOMER Pro is quite accurate except in the months of October, November, and December, whereas RETScreen Expert consistently overestimated the ratio, except in these three months. The information obtained from the simulation can be useful for investigating the characteristics of the photovoltaic system under different conditions (temperature, insolation) or the impact of cell technology. Energy generation predicted by simulation gives an idea of power plant performance when precise measurements of radiation, power and energy exported under varying environmental conditions are available. Several physical and statistical models have been established to predict the output and overall performance of photovoltaic systems (Tsoutsos et al., 2005; Tian et al., 2009). The results shown here should guide researchers and engineers who are modeling and planning solar photovoltaic power projects. Sizing is a crucial aspect of solar power plant design. Modeling focuses not only on sizing but also on optimization for operation under variable meteorological conditions.

In Fig. 22, the monthly average photovoltaic system efficiency for 2018 varied from 10.34% in July to 15.04% in November, due

to temperature effects. Inverter efficiency varied from 94% in July to 98.23% in February.

5.7. Influence of temperature on the photovoltaic system

To explain the influence of temperature on module (and hence power plant) efficiency, we used RETScreen and HOMER Pro to simulate the power capacity of a 20 MW power plant built with micro-crystalline or thin-film solar cells. Thin-film cells reportedly perform well in the summer compared to crystalline silicon cells due to their low temperature coefficient (ElhadjSidi et al., 2016). The results of RETScreen simulations with poly-crystalline silicon cells (Yingli Solar YL254-29b) replaced by mono-crystalline (Canadian Solar CSK 56 295 MS) or thin film (First Solar series 4 107 Cd/Te - FS-4105 A) cells under the same conditions are shown in Table 10. The thin-film cells are clearly expected to perform better than either crystalline silicon solar cell in hot climates, which has been confirmed elsewhere (ElhadjSidi et al., 2016). In addition, the capital cost of a large power plant using thin-film cells would be lower than one using poly-crystalline silicon cells.

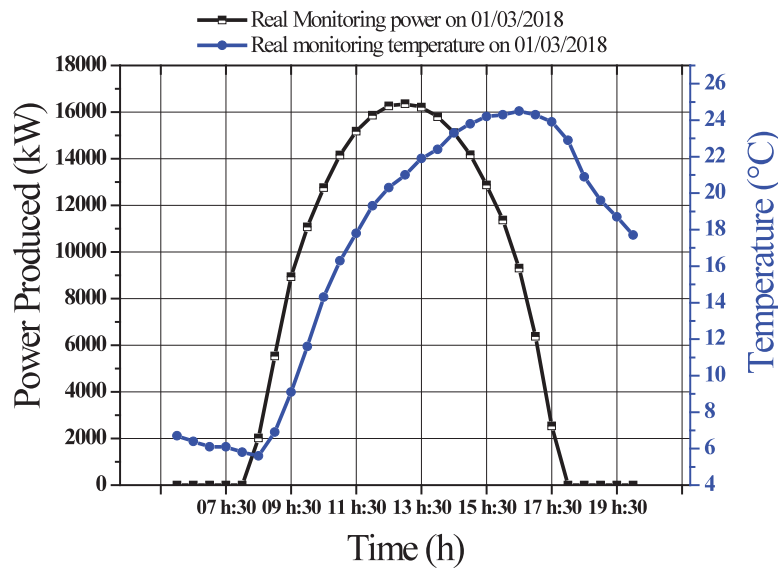


Fig. 15. Photovoltaic power output and ambient temperature measured on a typical summer day.

Table 10

Comparison of monthly photovoltaic electrical energy generation (MWh) simulated on HOMER Pro and RETScreen Expert for a 20 MW power plant operating in a hot climate.

Month	RETScreen Expert			HOMER Pro		
	Thin film ^a	Mono-crystalline ^b	Poly-crystalline ^c	Thin film	Mono-crystalline	Poly-crystalline
January	3535.8934	4080.0128	3480.096	2832.866	2630.407	2824.766
February	3362.9426	4386.1853	3285.161	2997.656	2765.494	2982.976
March	4096.0854	4286.1243	3969.518	3669.913	3354.576	3641.157
April	3896.1797	4100.2547	3751.558	3548.235	3219.980	3510.405
May	3902.9448	4032.3182	3732.318	3471.689	3130.906	3425.528
June	3790.4596	4085.875	3585.228	3172.108	2840.194	3121.276
July	3904.7411	2905.8547	3673.968	3401.284	3026.438	3341.015
August	3949.029	3014.6854	3715.633	3416.137	3038.213	3356.639
September	3660.6918	3256.3654	3472.225	3278.766	2931.863	3228.856
October	3574.3383	3149.2001	3437.677	2951.164	2685.214	2920.978
November	3248.4903	3358.2014	3167.7504	2693.460	2476.167	2676.271
December	3110.1138	3724.5684	3066.4521	2591.693	2408.362	2583.699
Total	44031.91	44132.82	42337.5855	38024.972	34507.814	37613.569

^aFirst Solar series 4 107 CdTe - FS-4105A.

^bMono-crystalline Canadian Solar CSK 56 295 MS.

^cYingli Solar YL254-29b.

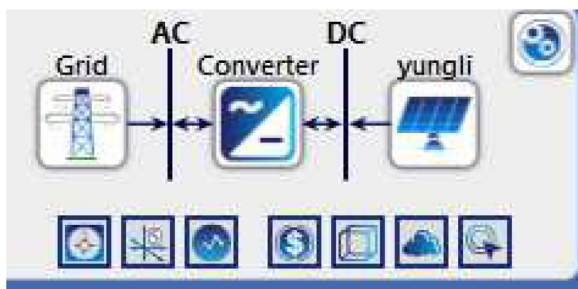


Fig. 16. System configuration as modeled by HOMER Pro.

5.7.1. Effect of temperature on photovoltaic cell efficiency

Ambient temperature and cell temperature display a linear relationship. The increase in module temperature causes the electrical power output to decrease (Yao et al., 2014).

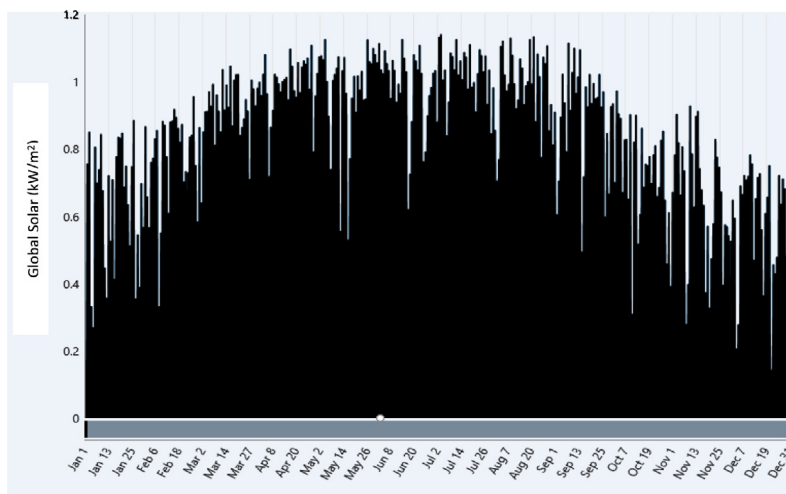
$$T_{cell} = T_{amb} + H \times (T_{nco} - 25) / 800 \quad (15)$$

where T_{cell} , T_{amb} are respectively the cell and ambient temperatures, H is irradiance in W/m^2 , and T_{nco} is the manufacturer-specified nominal cell operating temperature ($45^\circ C$).

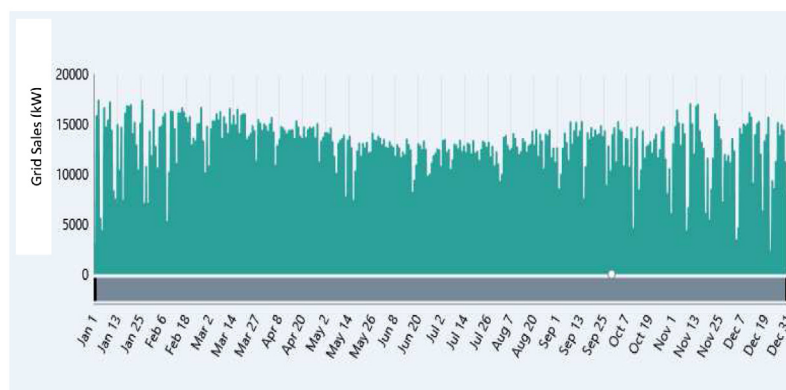
Monthly average ambient temperatures varied from $19.1^\circ C$ in January to $43.4^\circ C$ in July. The corresponding monthly average cell temperatures were $44.1^\circ C$ and $68.4^\circ C$. The curves are not perfectly symmetrical and are highly coherent with each other (Fig. 23).

The lower efficiencies measured in June, July and August can be attributed to temperature effects and solar technologies as indicated in Fig. 23 and Table 10. The negative slope of the efficiency versus temperature regression indicates that higher ambient temperature has an adverse effect on overall efficiency.

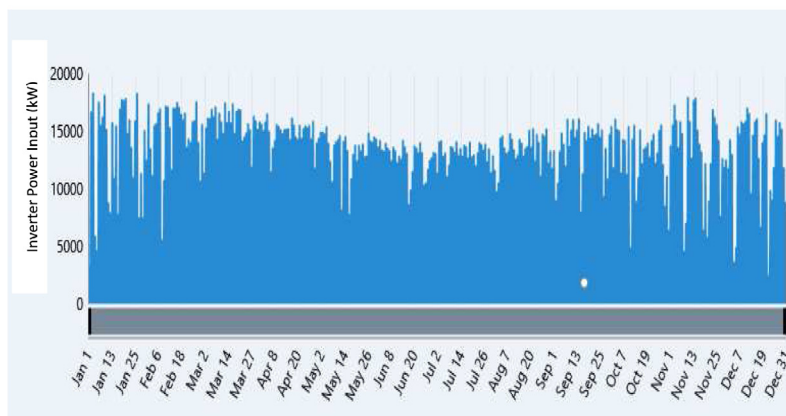
Real data and HOMER Pro calculations differ considerably (Fig. 24). The software appears to underestimate considerably the influences of temperature and panel technology. On a hot day such as July 27, 2018, the actual production was 6000 kW, while the HOMER Pro estimate was 14,000 kW. The temperature has a stronger effect on the efficiency of the Yingli YL254-29b polycrystalline silicon solar panel than was attributed in the software, which appears to be quite indifferent to high-precision meteorological data. Actual energy loss is more than 50% during peak hours on days when the panel temperature exceeds



17a – Total incident solar radiation calculated by HOMER Pro



17b – Solar electricity sales to the Grid as predicted by HOMER Pro



17c – Inverter power input calculated by HOMER Pro

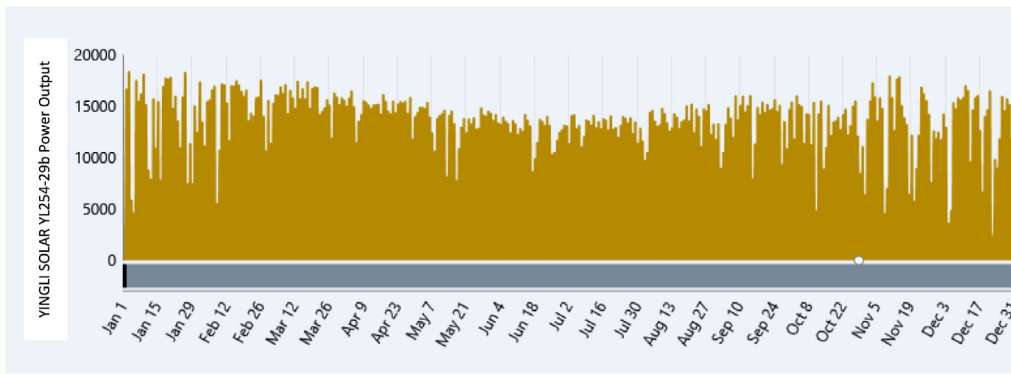
Fig. 17. HOMER Pro output results.

50 °C for the whole day, decreasing the power plant output. In some cases, for small application, PV/T system was indicated as one of the best ways to reduce the dependence of PV on temperature (Atmaca and Pektemir, 2019).

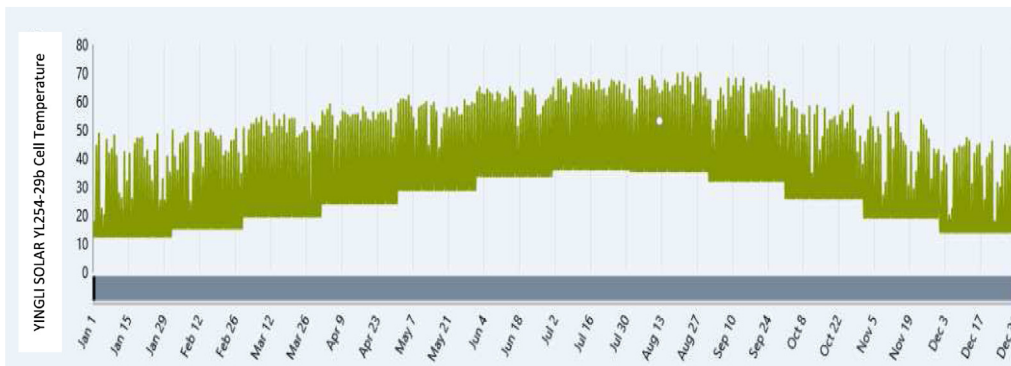
5.8. Photovoltaic forecasting and key indicators

Models that use forecasted irradiance like those that use forecasted wind to predict power output are gaining in popularity. Clouds and fog have the biggest influence on insolation,

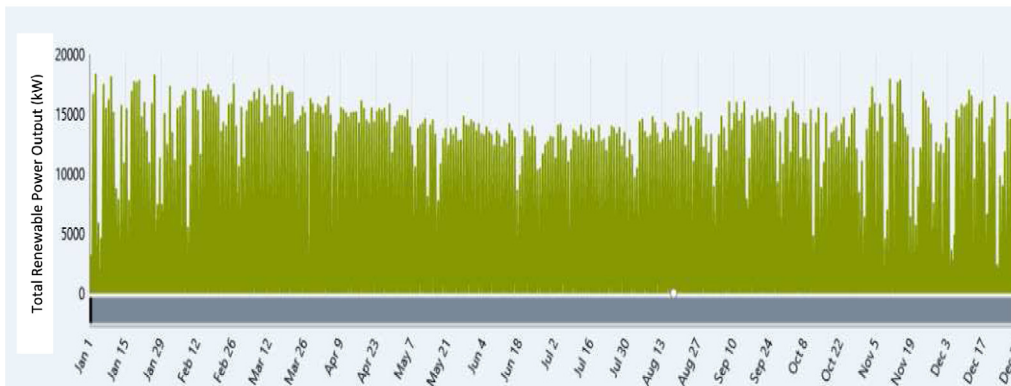
whereas temperature and cell technology affect power production on longer time scales. Specific molecules and aerosols in air also have an influence. Since the orientation and inclination of the photovoltaic panels are known, it is possible to forecast the peak power output on clear sky days. We used statistical analysis to validate photovoltaic forecasting by comparing the predictions with real data obtained by direct monitoring.



18a – Power output calculated by HOMER Pro



18b – Solar cell temperature calculated by HOMER Pro



18c – Total renewable energy output calculated by HOMER Pro

Fig. 18. Output power results predicted by HOMER Pro.

5.8.1. Statistical analysis of power output forecasting

The statistical indicators used to compare model results to real data were the mean bias error (MBE), root mean square error (RMSE), mean percentage error (MPE) and the t statistic as defined in the literature (Tarhan and Sari, 2005). The MBE provides an assessment of the long-term performance of the simulation. A positive value indicates overestimation, a negative value indicates under-estimation by the simulation software, the smaller the absolute value, the greater the exactness. The RMSE provides an assessment of the short-term performance of the proposed model by allowing a term-by-term comparison of the actual deviation between predicted and measured values. The MBE and RMSE both provide a rational basis for comparison, but no objective indicator of the statistical significance of deviations of model predictions from actual measurements (Stone, 1993; Padmavathi and Daniel,

2013). The t statistic allows us to state with a specified level of confidence whether the model predictions are accurate or not (Sundaram et al., 2015; Yao et al., 2014).

5.8.2. Root mean square error (RMSE)

The root mean square error can be computed using the following equation. Its value is always positive, zero meaning perfect prediction accuracy (never achieved in practice) (Stone, 1993; Padmavathi and Daniel, 2013).

$$RMSE = \sqrt{\frac{1}{n} \sum_{i=1}^n (c_i - m_i)^2} \tag{16}$$

c_i Energy capacity installed.
 m_i Energy measured.

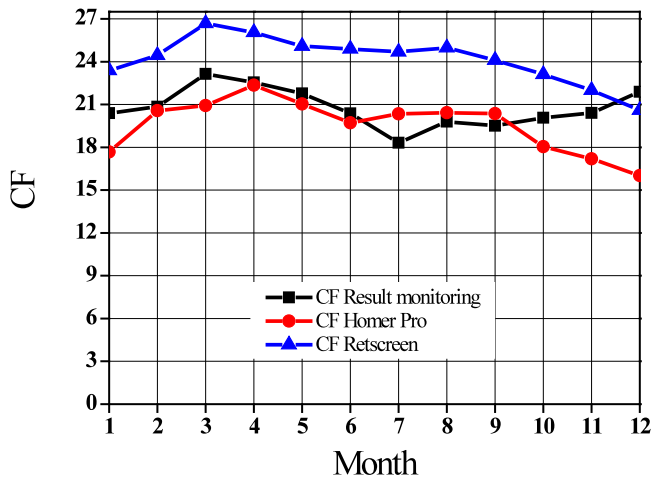


Fig. 19. Capacity factor during the year 2018, based on real data, HOMER Pro and RETScreen Expert.

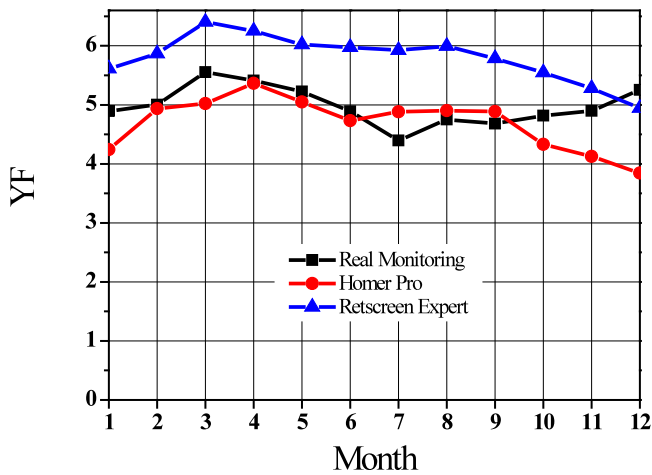


Fig. 20. Y_r during the year 2018, based on real data, HOMER Pro and RETScreen Expert.

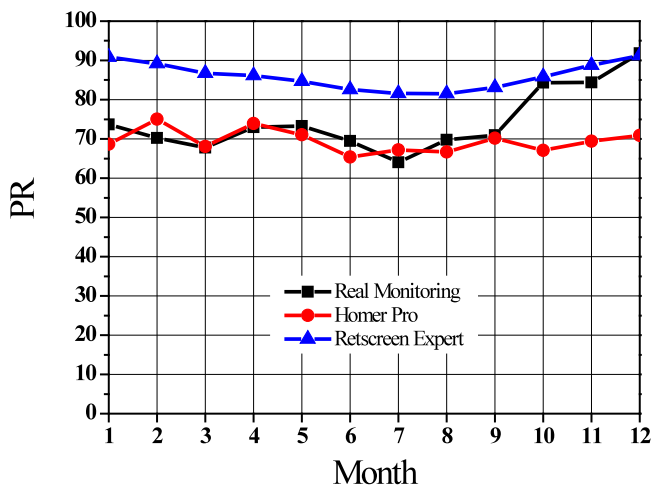


Fig. 21. Performance ratio during the year 2018, based on real data, HOMER Pro and RETScreen Expert.

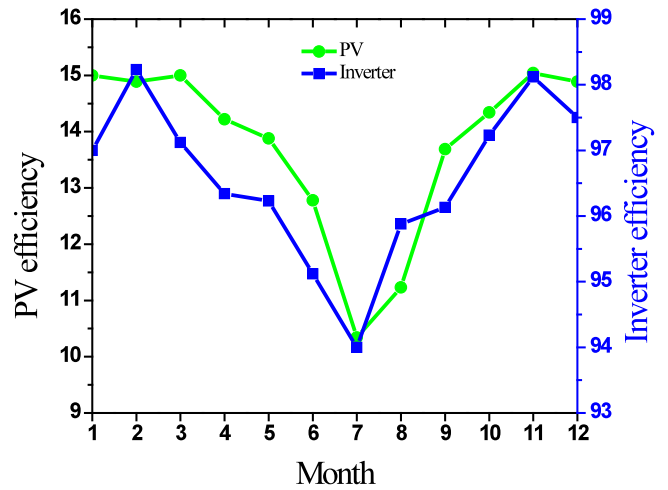


Fig. 22. Power plant photovoltaic and inverter efficiency.

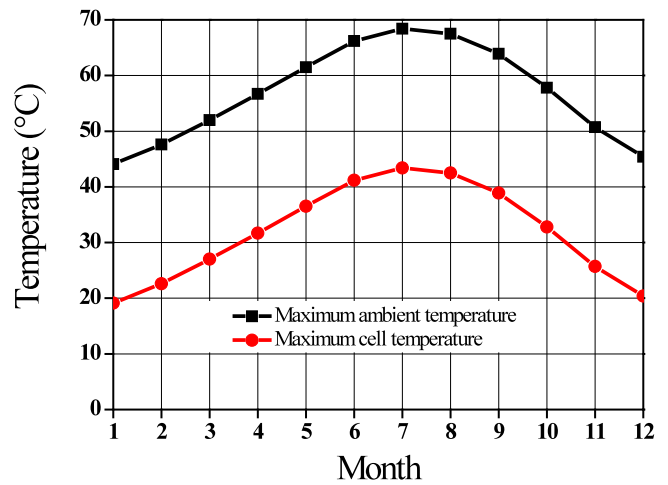


Fig. 23. Ambient temperature and photovoltaic cell temperature (monthly averages).

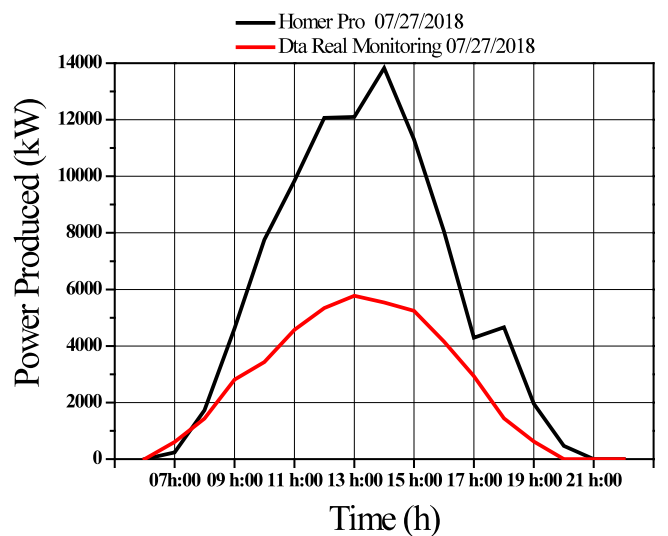


Fig. 24. Influence of temperature on electricity production.

Table 11

Accuracy of HOMER Pro and RETScreen Expert at predicting power output of hot climate photovoltaic power plant.

Software	RMSE	MPE (%)	t statistic	MBE
HOMER Pro	351.1	−0.00095	3.75	−176.88
RETScreen Expert	566.7	0.0016	6.12	497.80

5.8.3. Mean bias error (MBE)

The mean bias error is expressed as follows (Stone, 1993; Padmavathi and Daniel, 2013)

$$MBE = \frac{1}{n} \sum_{i=1}^n (c_i - m_i) \quad (17)$$

An MBE of zero would indicate that all values calculated by the model were identical to the measured values throughout the period of study, which never occurs in practice (Oliveira et al., 2002).

5.8.4. The t statistic method

The statistical significance of the deviations of the predicted values from the measured values, that is, the level of confidence with which it can be said that such deviations are systematic and a characteristic of the comparison under study (Stone, 1993), is evaluated using the t statistic (Oliveira et al., 2002). This can be computed using both the RMSE and MBE and considers the dispersion of the results, which is neglected when these error calculations are used separately. The smaller the t value, the more accurate are the predictions.

$$t - \text{stat} = \sqrt{\frac{(n - 1) MBE^2}{RMSE^2 - MBE^2}} \quad (18)$$

5.8.5. Mean percentage error (MPE)

The mean percentage error is the percent deviation of the estimated monthly average daily energy values from the measured values. The equation is written as follows:

$$MPE = \sum_{i=1}^n E/n \quad (19)$$

The best regression values generated by RETScreen and HOMER PRO as predictors of the real-time performance of the 20 MW power plant are compared in Table 11.

Based on the t statistic, HOMER Pro was closer to the monitored values, but both simulations deviated from reality, by 14% for RETScreen and by 5% for HOMER PRO, both validated by the RMSE, MPE and MBE (Ma et al., 2021). HOMER Pro underestimated the annual production of electricity (MBE = −176.88) and RETScreen overestimated it (MBE = 497.80). These deviations between the actual data and the simulation results could be caused factors associated with the Adrar region such as dust accumulation (Enaganti et al., 2022), very hot desert climate most of the year, degradation of photovoltaic modules and inappropriate choice of solar cell technology. Degradation observed in fielded PV modules is higher in hot climatic zones, specifically in hot and dry zone, as compared to other climates (Omar et al., 2020; Bansal et al., 2021). The performance of a 2000 MW solar PV plant operating under the weather conditions in Kuwait, which is close to the weather of Adrar region, was simulated using Monte Carlo approach. The results showed, on average, that power generation was 13% lower in the summer period compared with the spring when the temperature is milder and solar production peaks (Alshawaf et al., 2020).

6. Conclusion

The performance of a grid-connected 20 MW photovoltaic power plant operating in a hot climate was characterized in terms of the influence of insolation, air temperature, solar cell technology of electricity production and yield. The performance of the power plant depended heavily on insolation and environmental conditions, especially temperature. The solar cell technology used likely contributed to underperformance. Real data showed that high temperatures negatively affect the behavior of polycrystalline silicon cells resulting in non-optimal operation in the Sahara Desert as the cell temperatures reach more than 60 °C during the hottest months and the electrical production capacity is reduced by more than 40%. Commercial software predicts better performance from thin film solar cells under hot climate conditions. The power plant could be made at least 5% more efficient with thin-film solar cells, which are less sensitive to temperature changes and cost less initially and are therefore more recommendable for photovoltaic power generation in hot climates like in southern Algeria and the MENA region in general. Commercial simulation tools are very useful for designing and sizing large-scale photovoltaic power projects. The impact of temperature effects, insolation, wind velocity and cell technology can be assessed by numerical simulations such as HOMER Pro and RETScreen Expert. HOMER Pro results were found very close to those recorded by real-time monitoring to predict total production of electricity. In our analysis of case study, HOMER Pro is very strong by making it easy to compare thousands of possibilities, investigating all potential combinations of system types and then categorizing the systems according to the selected optimization variable. This gives us the possibility to quantify the impact of variables other than our control, such as PV technologies solar cell impact, temperature, wind speed, solar radiation, and understand how the optimal system changes with these variations like in hot climates. Therefore, the total electrical energy provided by this hot climate power plant in Adrar region was 36363.88 MWh in 2018, only about 5.1% more than the amount predicted by HOMER Pro (34507.81 MWh) and 14% less than what was predicted by RETScreen Expert (42338.57 MWh). This underlines the performance of that Homer Pro in this specific case of hot climate. The errors in the predictions are due mainly to the inaccuracies of the weather databases used by the simulators, especially for the hot summer months. Based on the t statistic, HOMER Pro was the better of the two simulators, although neither was very accurate. This analysis of the performance of the hot climate power plant suggests major design errors to be avoided in similar photovoltaic power projects in MENA regions and in hot climates anywhere in the world. It also shows that large-scale photovoltaic power plants are feasible and very competitive in such regions and that renewable energy programs initiated by MENA countries are justified. These results show that the performance of such systems does not depend exclusively on insolation but also on solar panel technology, temperature, and environmental conditions of operation.

Nomenclature

PV	Photovoltaic
HOMER	Pro Hybrid Optimization Model for Electric Renewables.
RETScreen	Energetic software developed by resources Canada.
GIS	Geographic Information System

GIPV	Grid Interactive PV
GHG	Greenhouse Gas Emissions
IEC	International Electrotechnical Commission
IRENA	International Renewable Energy Agency
SCADA	Supervisory control and data acquisition.
CIS	Copper Indium Selenide
CdTe	Cadmium Telluride
C-Si	Crystalline Silicon
GHG	Greenhouse gas
SKTM	Society Karaba Takkat Moutajadede (Company of renewable energies).
NOCT	Nominal operating cell temperature
MPPT	Maximum power point tracker
MENA	Middle East and North Africa
Yf	Final yield Rating.
Yr	Reference yield.
P_{rated}	Rated power
E_{AC}	Actual array output energy
PR	Performance ratio
CP	Capacity factor.
T_{cell}	Cell temperature.
T_{amb}	Ambient temperature.
T_{nco}	Manufacturer-specified nominal cell operating temperature.
H	Derived array plane insolation in Wh/m^2
G_{ref}	Reference irradiance at STC (1000 W/m^2)
E_{DC}	Energy delivered pb PV on DC
GHI	Global horizontal irradiance
DNI	Direct normal irradiance
RMSE	Root mean square error.
MPE	Mean percentage error.
MBE	Mean bias error.
t-stat	t statistic.

CRedit authorship contribution statement

Said Bentouba: Conception and design of study, Acquisition of data, Analysis and/or interpretation of data, Writing - original draft, Writing - review & editing. **Mahmoud Bourouis:** Conception and design of study, Analysis and/or interpretation of data, Writing - original draft, Writing - review & editing. **Nadjet Zioui:** Conception and design of study, Analysis and/or interpretation of data, Writing - original draft, Writing - review & editing. **Arumugam Pirashanthan:** Writing - original draft, Writing - original draft. **Dhayalan Velauthapillai:** Conception and design of study, Writing - original draft, Writing - review & editing.

Declaration of competing interest

The authors declare that they have no known competing financial interests or personal relationships that could have appeared to influence the work reported in this paper.

Acknowledgments

The authors gratefully acknowledge the Algerian Company of Electricity and Renewable Energy SKTM (Shariket Kahraba wa Taket Moutadjadida) for collaborating in this investigation and the supply of design and real monitoring data of the power plant. All authors approved the version of the manuscript to be published.

References

- Al-Badi, A.H., 2018. Measured performance evaluation of a 1.4 kW grid connected desert type PV in Oman. *Energy Sustain. Dev.* 47, 107–113.
- Algeria Ministry of Energy. 2021. <http://www.energy.gov.dz/francais>.
- Alshawaf, M., Poudineh, R., Alhajari, N.S., 2020. Solar PV in Kuwait: The effect of ambient temperature and sandstorms on output variability and uncertainty. *Renew. Sustain. Energy Rev.* 134.
- Atmaca, M., Pektemir, I.Z., 2019. An investigation on the effect of the total efficiency of water and air used together as a working fluid in the photovoltaic thermal systems. *Processes* 7.
- Bansal, N., Pany, P., Singh, G., 2021. Visual degradation and performance evaluation of utility scale solar photovoltaic power plant in hot and dry climate in western India. *Case Stud. Therm. Eng.* 26.
- Bentouba, S., Bourouis, M., 2016. Feasibility study of a wind-photovoltaic hybrid power generation system for a remote area in the extreme south of Algeria. *Appl. Therm. Eng.* 99, 713–719.
- Besarati, S.M., Padilla, R.V., Goswami, D.Y., Stefanakos, E., 2013. The potential of harnessing solar radiation in Iran: Generating solar maps and viability study of PV power plants. *Renew. Energy* 53, 193–199.
- Cabrera-Tobar, A., Bullich-Massagué, E., Aragüés-Peñalba, M., Gomis-Bellmunt, O., 2016a. Review of advanced grid requirements for the integration of large-scale photovoltaic power plants in the transmission system. *Renew. Sustain. Energy Rev.* 62, 971–987.
- Cabrera-Tobar, A., Bullich-Massagué, E., Aragüés-Peñalba, M., Gomis-Bellmunt, O., 2016b. Topologies for large scale photovoltaic power plants. *Renew. Sustain. Energy Rev.* 59, 309–319.
- Cazzaniga, R., Cicu, M., Rosa-Clot, M., Rosa-Clot, P., Ventura, C., 2018. Floating photovoltaic plants: Performance analysis and design solutions. *Renew. Sustain. Energy Rev.* 81, 1730–1741.
- Ebaid, M.S.Y., Hammad, M., Alghamdi, T., 2015. Thermo economic analysis of PV and hydrogen gas turbine hybrid power plant of 100 MW power output. *Int. J. Hydrogen Energy* 40, 12120–12143.
- ElhadjSidi, C.E., Ndiaye, M.L., El Bah, M., Mbodji, A., Ndiaye, P.A., 2016. Performance analysis of the first large-scale (15 MWp) grid-connected photovoltaic plant in Mauritania. *Energy Convers. Manage.* 119, 411–421.
- Enaganti, K.P., Bhattacharjee, A., Ghosh, A., Chanchangi, N.Y., Chakraborty, C., Mallick, T.K., Goel, S., 2022. Experimental investigations for dust build-up on low-iron glass exterior and its effects on the performance of solar PV systems. *Energy* 239.
- Guerrero-Lemus, R., Cañadillas-Ramallo, D., Reindl, T., Valle-Feijóo, J.M., 2019. A simple big data methodology and analysis of the specific yield of all PV power plants in a power system over a long time period. *Renew. Sustain. Energy Rev.* 107, 123–132.
- Gürtürk, M., 2019. Economic feasibility of solar power plants based on PV module with leveled cost analysis. *Energy* 171, 866–878.
- Hammad, B., Al-Abed, M., Al-Ghandoor, A., Al-Sardeah, A., Al-Bashir, A., 2018. Modeling and analysis of dust and temperature effects on photovoltaic systems performance and optimal cleaning frequency: Jordan case study. *Renew. Sustain. Energy Rev.* 82, 2218–2234.
- IRENA, 2021. Renewable Capacity Statistics 2021. International Renewable Energy Agency (IRENA), Abu Dhabi.
- Kumar, N.M., Gupta, R.P., Mathew, M., Jayakumar, A., Singh, N.K., 2019. Performance, energy loss, and degradation prediction of roof-integrated crystalline solar PV system installed in Northern India. *Case Stud. Therm. Eng.* 13, 100409.
- Kumar, M., Kumar, T.A., 2017. Performance assessment and degradation analysis of solar photovoltaic technologies: A review. *Renew. Sustain. Energy Rev.* 78, 554–587.
- Kumar, N.M., Malvoni, M., 2019. A preliminary study of the degradation of large-scale c-Si photovoltaic system under four years of operation in semi-arid climates. *Results Phys.* 12, 1395–1397.
- Kumar, B.S., Sudhakar, K., 2015. Performance evaluation of 10 MW grid connected solar photovoltaic power plant in India. *Energy Rep.* 1, 184–192.
- Ma, Y., Lv, Q., Zhang, R., Zhang, Z., Zhu, H., Yin, W., 2021. Short-term photovoltaic power forecasting method based on irradiance correction and error forecasting. *Energy Rep.* 7, 5495–5509.
- Marion, B., Adelstein, J., Boyle, K., Hayden, H., Hammond, B., Fletcher, T., Canada, B., Narang, D., Kimber, A., Mitchell, L., Rich, G., Townsend, T., 2005. Performance parameters for grid-connected PV systems. In: Conference Record of the Thirty-First IEEE Photovoltaic Specialists Conference.
- Martín-Martínez, S., Cañas-Carretón, M., Honrubia-Escribano, A., Gómez-Lázaro, E., 2019. Performance evaluation of large solar photovoltaic power plants in Spain. *Energy Convers. Manage.* 183, 515–528.
- Necaibia, A., Bouraiou, A., Ziane, A., Sahouane, N., Mouhadjer, S., 2018. Analytical assessment of the outdoor performance and efficiency of grid-tied photovoltaic system under hot dry climate in the south of Algeria. *Energy Convers. Manage.* 171, 778–786.
- Oliveira, A.P., Escobedo, J.F., Machado, A.J., Soares, J., 2002. Correlation models of diffuse solar radiation applied to the city of São Paulo, Brazil. *Appl. Energy* 71, 59–73.

- Omar, N.I., Boukhattem, L., Oudrhiri, H.F., Bennouna, A., Oukennou, A., 2020. Outdoor performance analysis of different PV technologies under hot semi-arid climate. *Energy Rep.* 6 (6), 36–48.
- Padmavathi, K., Daniel, S.A., 2013. Performance analysis of a 3MWp grid connected solar photovoltaic power plant in India. *Energy Sustain. Dev.* 17, 615–625.
- Pavlović, T., Milosavljević, D., Radonjić, I., Pantić, L., Radivojević, A., Pavlović, M., 2013. Possibility of electricity generation using PV solar plants in Serbia. *Renew. Sustain. Energy Rev.* 20, 201–218.
- Pothecary, S., 2016. Solar to account for 30% of all generation capacity investment until 2040 – PV Magazine International. https://www.pv-magazine.com/2016/06/13/solar-to-account-for-30-of-all-generation-capacity-investment-until-2040_100024957/.
- Purohit, I., Purohit, P., 2018. Performance assessment of grid-interactive solar photovoltaic projects under India's national solar mission. *Appl. Energy* 222, 25–41.
- Radziemska, E., Klugmann, E., 2002. Thermally affected parameters of the current–voltage characteristics of silicon photocell. *Energy Convers. Manage.* 43 (14), 1889–1900.
- Rashwan, S.S., Shaaban, A.M., Al-Suliman, F., 2017. A comparative study of a small-scale solar PV power plant in Saudi Arabia. *Renew. Sustain. Energy Rev.* 80, 313–318.
- Rehman, S., Ahmed, M.A., Mohamed, M.H., Al-Sulaiman, F.A., 2017. Feasibility study of the grid connected 10MW installed capacity PV power plants in Saudi Arabia. *Renew. Sustain. Energy Rev.* 80, 319–329.
- Satsangi, K.P., Bhagwan, D.D., Sailable, A.K., Saxena, B.G.S., 2018. Performance analysis of grid interactive solar photovoltaic plant in India. *Energy Sustain. Dev.* 47, 9–16.
- Şenol, M., Abbasoğlu, S., Kükrerb, O., Babatunde, A.A., 2016. A guide in installing large-scale PV power plant for self-consumption mechanism. *Sol. Energy* 132, 518–537.
- SKTM, 2019. Shariket Kahrabawa Taket Moutadjadida. <http://www.sktm.dz/>.
- Stone, R.J., 1993. Improved statistical procedure for the evaluation of solar radiation estimation models. *Sol. Energy* 51, 289–291.
- Sundaram, S., Sarat, J., Babu, C., 2015. Performance evaluation and validation of 5MWp grid connected solar photovoltaic plant in South India. *Energy Convers. Manage.* 100, 429–439.
- Suresh Kumar, U., Manoharan, P.S., 2014. Economic analysis of hybrid power systems (PV/diesel) in different climatic zones of Tamil Nadu. *Energy Convers. Manage.* 80, 469–476.
- Susanto, J., Shahnia, F., Ludwig, D., 2018. A framework to technically evaluate integration of utility-scale photovoltaic plants to weak power distribution systems. *Appl. Energy* 231, 207–221.
- Tarhan, S., Sari, A., 2005. Model selection for global and diffuse radiation over the Central Black Sea (CBS) region of Turkey. *Energy Convers. Manage.* 46, 605–613.
- Tian, Y., Zhao, L., Meng, H., Sun, L., Yan, J., 2009. Estimation of un-used land potential for biofuels development in (the) People's Republic of China. *Appl. Energy* 86, 77–85.
- Tossa, Alain K., Soro, Y.M., Thiaw, L., Azoumah, Y., Sicot, Lionel, Yamegueu, D., Lishou, Claude, Coulibaly, Y., Razongles, Guillaume, 2016. Energy performance of different silicon photovoltaic technologies under hot and harsh climate. *Energy* 103, 261–270.
- Tsoutsos, T., Frantzeskaki, N., Gekas, V., 2005. Environmental impacts from the solar energy technologies. *Energy Policy* 33, 289–296.
- Vasel, A., Iakovidis, F., 2017. The effect of wind direction on the performance of solar PV plants. *Energy Convers. Manage.* 153, 455–461.
- Yadav, A.K., Sharma, V., Malik, H., Chandel, S.S., 2018. Daily array yield prediction of grid-interactive photovoltaic plant using relief attribute evaluator based Radial Basis Function Neural Network. *Renew. Sustain. Energy Rev.* 81 (2), 2115–2127.
- Yao, W., Li, Z., Wang, Y., Jiang, F., Hu, L., 2014. Evaluation of global solar radiation models for Shanghai, China. *Energy Convers. Manage.* 84, 597–612.